Development of Superhydrophobic Silica Derived from Agricultural Biomass Waste as an Eco-Friendly Corrosion Inhibitor via Ultrasonic Dip-Coating

Lisnawaty Simatupang[1], Ricky Andi Syahputra[2], Elfrida Ginting[3], Maryati Doloksaribu[4], Binsar Maruli Tua Pakpahan[5], Fransiskus Hottua Malau[6], Winri Imanuela Sihombing[7], Carlos Rewandesno Sitorus[8]

{lisnawaty@unimed.ac.id[1], rickyandi@unimed.ac.id[2] , elfridaginting@unimed.ac.id[3]}

Department of Chemistry, Faculty of Mathematics and Natural Sciences, Universitas Negeri Medan, Jl. Willem Iskandar Psr. V, Medan, Sumatera Utara 20221, Indonesia[1,2,3,6,7,8]
Department of Physics, Faculty of Mathematics and Natural Sciences, Universitas Negeri Medan, Jl. Willem Iskandar Psr. V, Medan, Sumatera Utara 20221, Indonesia[4]
Department of Mechanical Engineering, Faculty of Engineering, Universitas Negeri Medan, Jl. Willem Iskandar Psr. V, Medan, Sumatera Utara 20221, Indonesia[5]

Abstract. Corrosion of metal components poses a persistent challenge in various industries due to moisture and aggressive environments. This study presents the development of superhydrophobic silica coatings derived from agricultural biomass waste (rice husk, corncob, and sugarcane bagasse) as eco-friendly corrosion inhibitors for mild steel. Silica was extracted via a sol–gel method after acid–alkali treatment and thermal calcination, then modified with trimethylchlorosilane (TMCS) to enhance hydrophobicity. The functionalized silica was applied onto steel substrates through ultrasonic dip-coating. Characterization using FTIR and XRD confirmed silanol functionalization and the amorphous structure of the silica. The coatings exhibited water contact angles above 150° and sliding angles below 10°, confirming superhydrophobicity. Corrosion tests in 15% HCl and 3.5% NaCl media showed a significant reduction in corrosion rate, achieving up to 92.8% inhibition efficiency at 5.0% silica concentration. These results suggest that biomass-derived silica provides a sustainable and high-performance solution for corrosion-resistant coatings.

Keywords: superhydrophobic silica, biomass waste, corrosion inhibitor, ultrasonic dip-coating, sol-gel synthesis.

1 Introduction

Corrosion of metallic structures represents a critical issue in industrial sectors such as construction, transportation, and energy, causing significant economic losses, structural failures, and safety concerns [1], [2]. In humid tropical countries like Indonesia, where relative humidity frequently exceeds 80%, metals are highly susceptible to degradation, leading to shortened

ICIESC 2025, September 16, Medan, Indonesia

DOI 10.4108/eai.16-9-2025.2361108

service life and increased maintenance costs [3]. The global cost of corrosion underscores the urgent need for effective and sustainable mitigation strategies.

Conventional corrosion inhibitors, particularly chromates and phosphates, have been widely adopted due to their strong protective performance. However, these compounds are toxic, poorly biodegradable, and increasingly restricted under environmental regulations [4]. This situation drives the search for eco-friendly alternatives. One promising approach is the development of superhydrophobic coatings, which can act as physical barriers by preventing water penetration and suppressing electrochemical reactions on metal [5], [6].

A surface is classified as superhydrophobic when its water contact angle (WCA) exceeds 150° and the sliding angle (SA) remains below 10°, enabling water droplets to roll off easily and removing corrosive species [7], [8]. Silica nanoparticles are frequently employed in such coatings owing to their abundance, stability, and ease of surface modification [9], [10]. Functionalization with trimethylchlorosilane (TMCS) effectively replaces surface hydroxyl groups with hydrophobic $–CH_3$ moieties, lowering surface energy while being less hazardous and more cost-efficient than fluorinated silanes [11], [12].

Despite the effectiveness of silica derived from commercial precursors such as tetraethyl orthosilicate (TEOS), their cost and non-renewable origin limit scalability. Agricultural biomass residues (including rice husk, corncob, sugarcane bagasse, and coconut husk) represent a sustainable and low-cost silica source [13], [14], [15]. Rice husk alone contains up to 20% silica, with potential yields exceeding 90% after acid–alkali treatment and calcination [16], [17]. Indonesia, as one of the world's largest rice producers, generates millions of tons of husk annually, much of which remains underutilized (BPS, 2023) [18]. Transforming this waste into high-value silica aligns with circular economy principles and provides a dual solution to waste management and corrosion protection [19], [20].

For effective coating deposition, uniformity and adhesion are critical. Ultrasonic-assisted dip-coating has emerged as a powerful method to enhance nanoparticle dispersion, improve coating homogeneity, and ensure robust bonding with metallic substrates [21], [22]. Recent studies demonstrated that silica-based ultrasonic coatings derived from volcanic ash or silica composites significantly enhance corrosion resistance in aggressive media [23], [24].

Building upon these advances, this study focuses on the synthesis of superhydrophobic silica coatings derived from rice husk, corncob, and sugarcane bagasse through a sol–gel route followed by TMCS functionalization. The coatings were applied to mild steel substrates using ultrasonic dip-coating, and their physicochemical properties were characterized via FTIR, XRD, and SEM-EDS. Corrosion resistance was evaluated in 15% HCl and 3.5% NaCl solutions using the weight loss method. This research contributes to the development of sustainable, high-performance, and environmentally friendly anti-corrosion materials by integrating agricultural waste valorization, surface functionalization, and advanced coating technology

2 Experimental

2.1 Materials

Agricultural biomass, namely rice husk (RH), corncob (CC), and sugarcane bagasse (SB), was collected from local sources in North Sumatra, Indonesia. Volcanic ash from Mount Sinabung (Namanteran Village, Karo Regency) was also included as a comparative silica source. All biomass samples were washed, dried, and stored prior to use. Analytical-grade reagents included sodium hydroxide (NaOH, ≥98%), hydrochloric acid (HCl, 37%), and sodium chloride (NaCl), all obtained from E-Merck. Trimethylchlorosilane (TMCS, ≥99%) and xylene (≥99%) were purchased from Sigma-Aldrich. Mild steel plates (3 cm × 3 cm × 3 mm, low-carbon steel) were used as the corrosion substrates. Supporting materials included velvet cloth, sandpaper, iron paint (ABC), Autosol metal polish, and demineralized water. All chemicals were used without further purification..

2.2 Equipment and Instrumentation

This study employed various laboratory equipment and analytical instruments to support synthesis, coating, and characterization processes. The main equipment included an ultrasonic homogenizer (OMNI SONIC Ruptor 400, 135 W, 42 kHz), ultrasonic bath (BANDELIN BactoSonic Type BS 14.2, 800 W, 40 kHz), furnace (Gallenkamp Hotspot), oven (Memmert® UO55), hot plate stirrer (Thermo Fisher Scientific), vacuum pump (Tasco-150SB-220), desiccator, 200 mesh sieve, analytical balance, mortar and pestle, and laser cutting tools. Analytical instruments used were Fourier Transform Infrared Spectroscopy (FTIR, Shimadzu IRTracer-100), X-ray Diffraction (XRD, Bruker D8 Advance Eco, Bragg–Brentano geometry), and Scanning Electron Microscopy with Energy Dispersive X-ray Spectroscopy (SEM-EDS, Zeiss EPOMH 10).

2.3 Silica Extraction from Biomass Waste

Each biomass type (RH, CC, SB) was washed with distilled water and dried at 80 °C. The dried samples were carbonized in a muffle furnace at 500–700 °C for 4 h to obtain ash. To remove metallic impurities, the ash was soaked in 12 M HCl for 24 h and rinsed thoroughly with distilled water until neutral. The demineralized ash was then reacted with 8 M NaOH under reflux to extract sodium silicate. After cooling and filtration, gelation was induced by adding 3 M HCl dropwise at 40 °C until the pH reached ~7, forming a silica gel. The gel was washed, dried at 120 °C, and ground into fine powder (200 mesh).

2.4 Surface Modification of Silica

Surface functionalization was performed by dispersing silica powder in xylene at concentrations ranging from 1.0 to 5.0% (v/v). The dispersion was stirred at 130 °C for 1 h to ensure uniform mixing. TMCS (8% v/v) was then added dropwise under acidic conditions (pH ≈ 2), and the reaction was maintained at 80 °C with continuous stirring (250 rpm) for 30 min. The TMCS-functionalized silica was collected, dried, and stored in sealed containers. Successful surface modification was confirmed by the presence of $–CH_3$ and –Si–C groups in FTIR spectra.

2.5 Coating Application via Ultrasonic Dip-Coating

Mild steel plates were polished with sandpaper, degreased with ethanol, and air-dried. Each plate was immersed in 20 mL of the TMCS-modified silica dispersion and subjected to ultrasonic dip-coating using a Branson ultrasonic bath (135 W, 42 kHz) for 25 min. After coating, the plates were dried at ambient temperature and weighed to determine their initial mass (Wi) before corrosion testing.

2.6 Corrosion Inhibition Efficiency Test

Coated steel plates were immersed in 15% HCl and 3.5% NaCl solutions for 96 h at room temperature. After immersion, the plates were dried and weighed to obtain the final mass (Wf). The corrosion rate (CR) was calculated using the weight loss method:

$$\mathrm{CR(mm/year)} = \frac{(\mathrm{Wi} - \mathrm{Wf}) \times 87.6}{\rho \; x \; A \; x \; T} \tag{1}$$

where Wi is the initial weight (g), Wf the final weight (g), ρ the density of metal (g/cm³), A the surface area (cm²), and t the immersion time (h).

The inhibition efficiency (η) was determined using:

$$\eta\,(\%) = \frac{\left(CR_{Blank} - \; CR_{Sample}\right)}{CR_{Blank}} \; x \; 100\% \tag{2}$$

Post-immersion analyses were performed using XRD and SEM-EDX to observe surface morphology and structural changes due to corrosion.

2.7 Data Analysis

Experimental data were analyzed quantitatively to evaluate the effectiveness of TMCS-modified silica as a corrosion inhibitor. Parameters analyzed included corrosion rate, inhibition efficiency, water contact angle, sliding angle, and coating adhesion strength (ASTM D4541). Qualitative analyses from FTIR, XRD, SEM-EDX, and BET confirmed successful synthesis and modification. Results were presented in tables and figures to support interpretation and conclusions.

3 Results and Discussion

3.1 Silica Extraction from Agricultural Biomass

The silica extraction process from agricultural biomass involved several critical steps, including washing, drying, carbonization, and calcination, to isolate high-purity silica ash. Washing was essential to remove surface impurities and inorganic contaminants. Dried biomass samples (rice husk, corncob, and sugarcane bagasse) were calcined in a muffle furnace at 700 °C for 6 h with a heating rate of 5 °C/min. At this temperature, organic components such as lignin and cellulose decomposed, leaving silica-rich ash. Rice husk yielded the highest silica content (95.41%), followed by corncob (66.64%) and sugarcane bagasse (63.52%). The ash from rice husk appeared bright white, indicating high purity, while corncob and sugarcane bagasse ashes were greyish, suggesting residual carbon or mineral content (Fig. 1).

Fig. 1. (a) Drying process of biomass: (a1) rice husk, (a2) corncob, (a3) sugarcane bagasse; (b) Ash appearance post-calcination: (b1) rice husk, (b2) corncob, (b3) sugarcane bagasse.

To enhance purity, acid leaching with 6 M HCl for 24 h was conducted to eliminate residual oxides. The ash was rinsed with deionized water until neutral pH was reached (Fig. 2a–b). Subsequently, the neutralized ash was treated with 8 M NaOH to form sodium silicate (Na_2SiO_3), producing a dense slurry (Fig. 2c). Rice husk yielded a clearer sodium silicate solution than corncob and sugarcane bagasse, indicating higher solubility and precursor quality (Fig. 3).

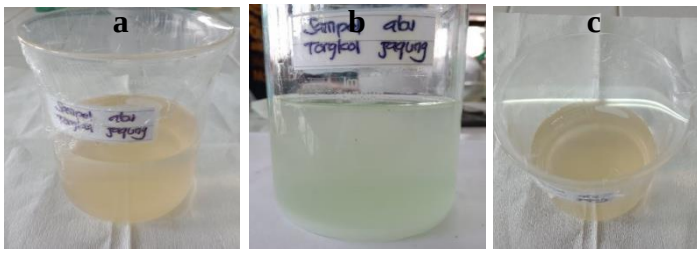

Fig. 2. (a) Acid demineralization in 6 M HCl, (b) Neutralization with deionized water, (c) Sodium silicate slurry formation.

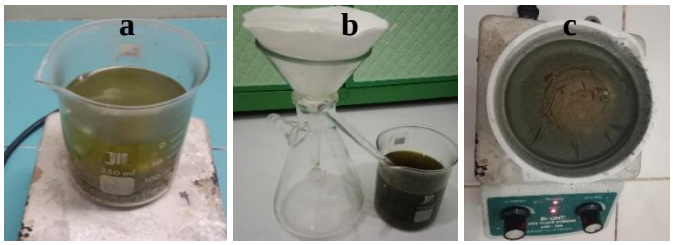

Fig. 3. Sodium silicate solutions obtained from (a) rice husk, (b) corncob, and (c) sugarcane bagasse.

Silica gel was produced by gradually acidifying the sodium silicate solution with 3 M HCl at 40 °C, promoting condensation of Si–OH groups into Si–O–Si linkages. The gel was filtered, washed, dried at 120 °C, and milled to fine powders (Fig. 4). Rice husk-derived silica showed the most uniform morphology and lowest residual moisture, making it the most promising precursor.

Fig. 4. Final dried and milled silica powders derived from each biomass source.

3.2 Characterization and Yield Analysis of Silica from Biomass Waste

Silica powders from rice husk, corncob, and sugarcane bagasse appeared as bright white fine powders with uniform homogeneity (Fig. 5). However, the silica yield differed significantly: rice husk provided 95.41%, corncob 66.64%, and sugarcane bagasse 63.52%.

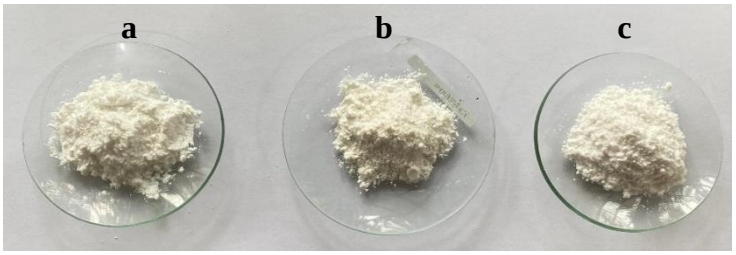

Fig. 5. Dried and milled silica powders from (a) corncob, (b) rice husk, and (c) sugarcane bagasse.

The higher yield of rice husk correlates with its naturally high silica content (>90%), while the lower yields of corncob and sugarcane bagasse reflect their heterogeneous distribution of silica. Higher silica yield enhances the probability of forming dense Si–O–Si networks during gelation, thereby increasing the number of active silanol groups for subsequent modification.

Experimental yields were compared with literature data (Table 1). Rice husk-derived silica (95.41%) aligned with reported recoveries of 90–99% [13], [17]. Corncob silica (66.64%) and sugarcane bagasse silica (63.52%) were consistent with reported ranges of 67.41% and 50–73%, respectively [15], [25].

Table 1. Comparison of experimental silica yield with literature values.

No.	Biomass Source	Experimental Yield (%)	Literature Yield (%)	References
1	Rice husk silica (RHS)	95.41	90–99	[13], [17]
2	Corncob silica	66.64	67.41	[25]

	(CCS)			
3	Sugarcane bagasse silica (SBS)	63.52	50–73	[15]

The consistency between experimental and literature values validates the robustness of the sol–gel protocol. Controlled pyrolysis temperature, acid pretreatment, and pH adjustment ensured reproducible extraction. Overall, rice husk was confirmed as the most promising silica precursor, providing superior yield and purity for advanced coating applications.

3.3 FTIR and XRD Analysis of Extracted Silica

3.3.1 Functional Group Identification via FTIR

The FTIR spectra of silica derived from rice husk (RHS), corncob (CCS), and sugarcane bagasse (SBS) exhibited similar patterns typical of amorphous silica. A broad absorption band at 3400–3450 cm^{-1} corresponded to O–H stretching vibrations of surface silanol groups (Si–OH), which act as reactive sites for silanization with trimethylchlorosilane (TMCS) [15], [16]. The intensity of this band reflects the availability of active sites for hydrophobization. Strong absorption at 1050–1100 cm^{-1}, attributed to asymmetric Si–O–Si stretching, confirmed the formation of siloxane linkages during sol–gel synthesis. Additional peaks near 790–800 cm^{-1} were assigned to symmetric Si–O vibrations, further validating the integrity of the siloxane network. These findings confirm that the extracted silica possesses the functional groups necessary for subsequent surface modification.

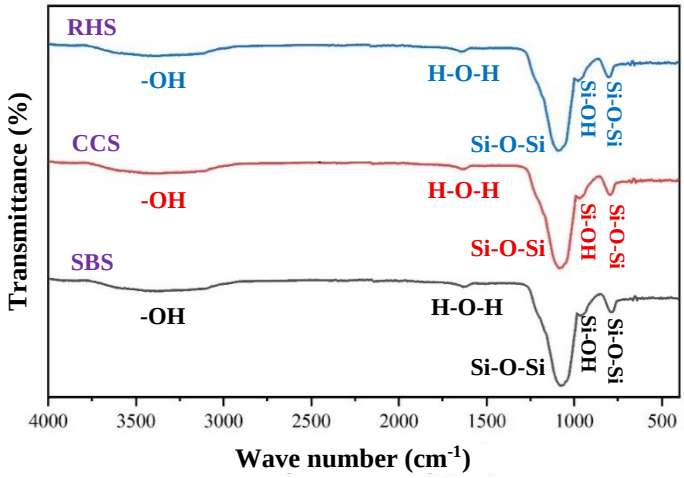

Fig. 6. FTIR spectra of silica extracted from rice husk (RHS), corncob (CCS), and sugarcane bagasse (SBS), showing silanol and siloxane groups.

3.3.2 Amorphous Structure Validation via XRD

The XRD patterns of RHS, CCS, and SBS (Fig. 7) revealed broad halos centered at $2\theta \approx 22°–23°$, characteristic of amorphous silica. The absence of sharp peaks corresponding to crystalline phases such as quartz indicated that the extracted materials lacked long-range atomic order. The

amorphous structure is advantageous for coating applications because it provides higher surface area, enhanced porosity, and reduced brittleness compared to crystalline silica.

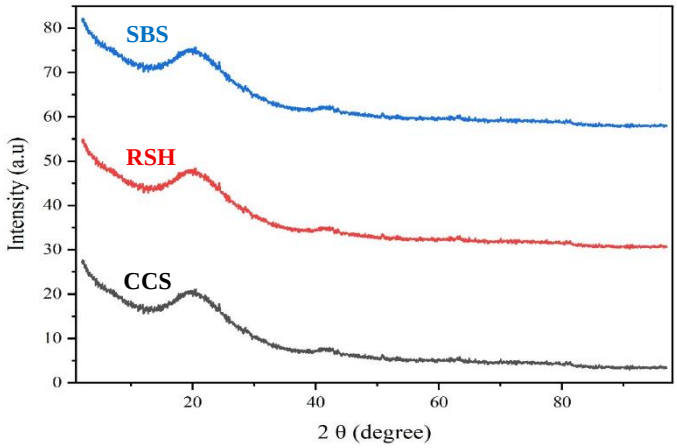

Fig. 7. XRD patterns of silica derived from RHS, CCS, and SBS, showing amorphous broad peaks at 2θ ≈ 22°.

3.3.3 Structure–Function Relationship for Superhydrophobic Coatings

The combined FTIR and XRD results confirm the suitability of the extracted silica for superhydrophobic coatings. The abundance of surface silanol groups provides high reactivity toward TMCS modification, while the amorphous structure ensures uniform dispersion in organic solvents. These complementary properties enable the formation of stable, nonpolar, and water-repellent coatings with enhanced durability and performance.

3.4 Surface Modification Effectiveness with TMCS

Following the successful extraction of high-purity silica from rice husk (RHS), corncob (CCS), and sugarcane bagasse (SBS), surface functionalization was conducted to transform the intrinsically hydrophilic silica into a superhydrophobic material. Native silica contains abundant surface silanol groups (–SiOH), which readily form hydrogen bonds with water molecules, making the material highly reactive to atmospheric moisture and unsuitable for anti-corrosion applications. The surface modification process with trimethylchlorosilane (TMCS) was employed to replace these polar functionalities with nonpolar methyl groups ($–CH_3$), thereby reducing surface energy and enhancing water repellency.

3.4.1 Silanol Substitution Mechanism

The surface modification reaction between silanol groups and TMCS can be described by the following equation:

$$\equiv Si–OH + Cl–Si(CH_3)_3 \rightarrow \equiv Si–O–Si(CH_3)_3 + HCl$$

This nucleophilic substitution reaction results in the formation of stable $Si–CH_3$ bonds while preserving the core siloxane (Si–O–Si) network of the silica. The reaction proceeds selectively

under mild acidic conditions and does not compromise the structural integrity of the silica framework.

3.4.2 Visual and Physical Indicators of Functionalization

Macroscopically, successful surface modification was accompanied by distinct changes in dispersion behavior and colorimetric cues. Prior to modification, silica dispersions in xylene at 130 °C exhibited a homogeneous, slightly turbid white appearance (Fig. 8a), indicating effective diffusion of silica particles without visible agglomeration. Upon gradual addition of TMCS at 80 °C, the solution transitioned to a pale green color (Fig. 8b), which served as a qualitative indicator of chemical interaction between TMCS and surface silanol groups. After reaction completion, the dispersion appeared milky-white with improved stability and no visible sedimentation (Fig. 8c), confirming successful surface functionalization and enhanced compatibility with the nonpolar xylene matrix.

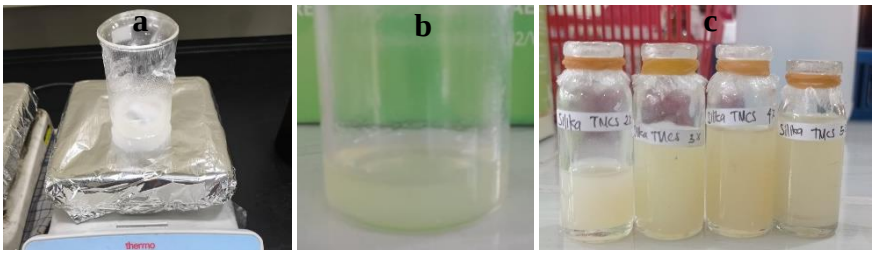

Fig. 8. Visual appearance of silica dispersions: (a) before TMCS addition (uniform white suspension), (b) during TMCS addition (pale green transition), and (c) after modification (milky-white stable dispersion).

3.4.3 Safety and By-Product Management

Although the TMCS–silanol reaction generates hydrochloric acid (HCl) as a by-product, the reaction system was designed to mitigate any residual acidity. Conducted in xylene, a nonpolar organic solvent, the system favors the volatilization of HCl due to its low solubility and high vapor pressure. The open reaction environment and elevated temperatures further promote safe dissipation of HCl vapors, preventing corrosive residues in the final coating formulation.

3.4.4 Functional Group Transformation Post-Modification

Fourier Transform Infrared Spectroscopy (FTIR) analysis of TMCS-functionalized silica revealed significant alterations in surface chemistry. Compared to unmodified silica, which displayed a strong absorption band at 3400–3450 cm^{-1} corresponding to O–H stretching vibrations of silanol groups, the modified samples exhibited a pronounced reduction of this band. Concurrently, new absorption bands emerged in the range of 1250–1270 cm^{-1} (deformation vibration of $–CH_3$ groups attached to Si) and 840–850 cm^{-1} (indicative of Si–C bond formation). These spectral features confirm that surface silanol groups were successfully replaced by nonpolar methyl groups while preserving the backbone Si–O–Si structure at 1050–1100 cm^{-1}.

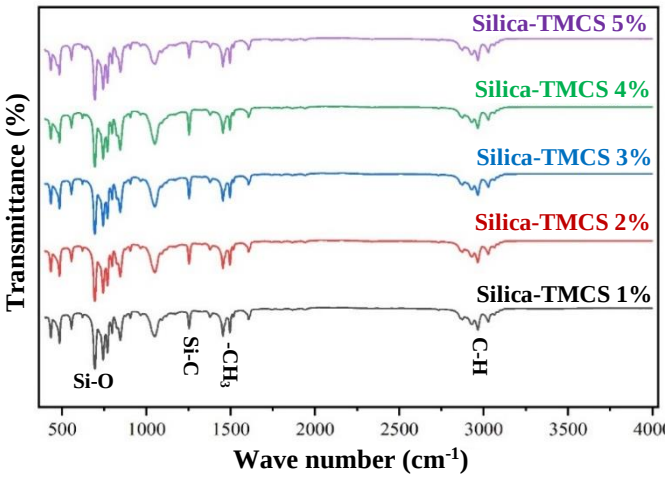

Fig. 9. FTIR spectra of TMCS-functionalized silica derived from rice husk (RHS), showing diminished –OH bands and the emergence of $–CH_3$ and Si–C peaks.

3.4.5 Enhancement of Surface Hydrophobicity

The substitution of hydrophilic –SiOH groups with nonpolar $–CH_3$ groups significantly transformed the surface properties of silica. This chemical transition disrupted the ability of the material to form hydrogen bonds with water, thereby reducing wettability and enabling superhydrophobic behavior. The disappearance of the –OH band along with the presence of Si–CH_3 and Si–C bands in the FTIR spectra validates this transformation. Additionally, the modified silica exhibited markedly improved dispersion stability in xylene, confirming a reduction in surface energy and increased affinity toward nonpolar solvents—an essential prerequisite for hydrophobic coating applications.

3.4.6 Structural Integrity and Dispersion Stability

Despite extensive surface modification, the persistent and symmetric Si–O–Si absorption bands demonstrate that the siloxane backbone remained intact, ensuring the mechanical and thermal integrity of the material. Furthermore, the TMCS-functionalized silica samples (RHS, CCS, SBS) maintained excellent colloidal stability, showing negligible agglomeration or sedimentation over time. This stability ensures reliable performance during downstream coating processes and supports the feasibility of using biomass-derived silica as a sustainable precursor for corrosion-resistant coatings.

3.5 Evaluation of Superhydrophobicity of Silica-TMCS Coating

The superhydrophobicity of silica–TMCS composite coatings was assessed through contact angle (CA) and sliding angle (SA) measurements on mild steel substrates. These parameters are widely recognized as quantitative indicators of water repellency, where a surface is classified as superhydrophobic if CA $\geq 150°$ and SA $\leq 10°$ [11], [12].

Table 2. Average water contact angle (°) on coated steel surfaces using silica–TMCS derived from different sources and concentrations.

Silica Source	Contact Angle (°)					
	0.0%	**1.0:8**	**2.0:8**	**3.0:8**	**4.0:8**	**5.0:8**
Control	68.2°	–	–	–	–	–
RHS	–	140.5°	151.7°	153.1°	152.9°	148.3°
CCS	–	136.7°	149.2°	150.8°	150.2°	146.5°
SBS	–	133.2°	146.5°	148.6°	148.1°	144.7°

All coatings demonstrated a substantial increase in CA compared to the uncoated control (68.2°), confirming enhanced hydrophobicity. Superhydrophobicity (CA ≥150° and SA ≤10°) was achieved at 2.0–3.0% concentrations for all silica sources, with RHS-based coatings yielding the highest performance (CA up to 153.1°).

At higher concentrations (≥4.0%), a slight decrease in CA was observed. This reduction is attributed to increased solution viscosity, leading to non-uniform layer deposition and reduced surface smoothness. Nonetheless, the coatings remained hydrophobic (CA >140°). SBS-derived silica, despite marked improvements, did not fully achieve superhydrophobicity (CA <150°), likely due to lower silanol density or less favorable particle morphology.

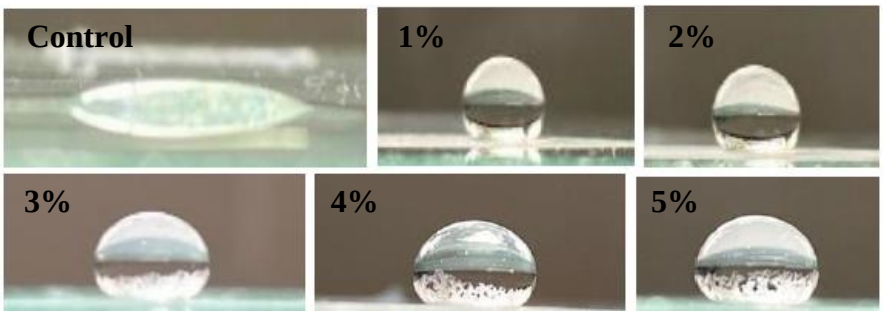

Fig. 10. Water contact angle and sliding angle measurements of silica–TMCS coatings prepared at different concentrations (control, 1–5%) and silica sources (a-f).

From a molecular perspective, the improved water repellency is primarily due to the grafting of nonpolar methyl groups (–CH_3) via TMCS, which replace hydrophilic silanol groups (–SiOH) and substantially lower the surface energy. Furthermore, the porous amorphous microstructure of the silica, as previously confirmed by XRD, facilitates the formation of hierarchical micro/nanostructures that trap air pockets. This synergistic effect enables the Cassie–Baxter wetting regime, where droplets rest on composite solid–air interfaces, thus minimizing adhesion and imparting robust superhydrophobic behavior.

3.6 Evaluation of Corrosion Inhibition Efficiency in Acidic and Saline Media

To evaluate the corrosion protection performance of the silica–TMCS composite coating, the ultrasonic dip-coating method was employed. This technique utilizes high-frequency (42 kHz) ultrasonic waves during immersion, facilitating the dispersion of silica particles, disrupting

agglomerates, and ensuring the formation of uniform and stable thin films on the metal substrate. Steel plates were immersed for 25 minutes in coating solutions of varying silica concentrations (1.0–5.0% v/v), followed by air drying. Coatings with 2.0–4.0% silica concentration produced uniform, thin white films on the metal surface.

Fig. 11. (a) Ultrasonic dip-coating process of silica–TMCS coatings on mild steel; (b) immersion of coated steel plates in corrosive media (15% HCl and 3.5% NaCl).

Subsequently, the corrosion resistance of the coated plates was assessed in two corrosive environments: 15% HCl (strong acid) and 3.5% NaCl (saline solution, simulating seawater conditions), over 96 hours at ambient temperature. The corrosion rate (CR) and inhibition efficiency (η) were calculated using the weight-loss method, and results were benchmarked against uncoated (control) plates.

Table 3. Corrosion rate and inhibition efficiency of silica–TMCS coatings in HCl and NaCl media.

Silica Concentration (%)	CR (HCl, mpy)	Efficiency (%)	CR (NaCl, mpy)	Efficiency (%)
Control (uncoated)	190.95	0	29.59	0
1.0%	148.67	22.14	6.38	78.45
2.0%	116.08	39.21	5.53	81.32
3.0%	85.04	55.47	3.61	87.79
4.0%	46.77	75.51	3.40	88.51
5.0%	37.42	80.41	2.13	92.82

As shown in Table 3, corrosion rates decreased significantly with increasing silica concentration in both environments. In 15% HCl, the corrosion rate decreased from 190.95 mpy (control) to 37.42 mpy at 5.0% concentration, corresponding to an inhibition efficiency of 80.41%. In 3.5% NaCl, inhibition efficiency was even higher, reaching 92.82% at 5.0%, with a corrosion rate of only 2.13 mpy. These results demonstrate the dual effectiveness of the coating, even under aggressive acidic conditions.

The enhanced protection is attributed to the formation of a dense superhydrophobic barrier that blocks the penetration of corrosive ions (H^+ and Cl^-). Functionalization with TMCS replaces hydrophilic silanol groups (Si–OH) with nonpolar methyl groups (Si–CH_3), drastically lowering surface energy and wettability, thereby minimizing electrolyte permeability.

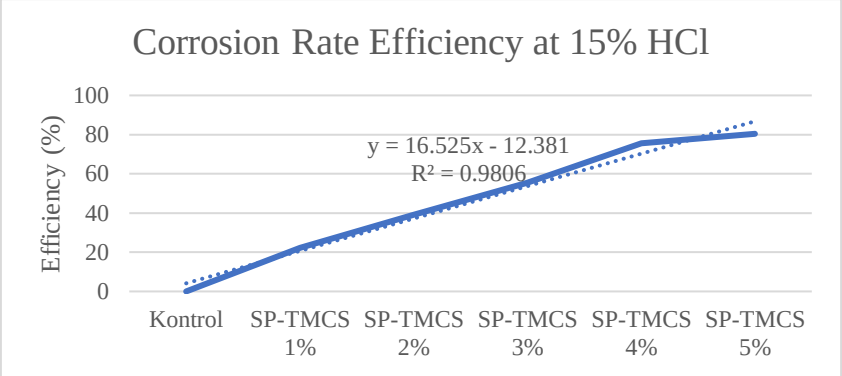

Fig. 12. Corrosion inhibition efficiency (%) of silica–TMCS coatings in 15% HCl solution.

As illustrated in Fig. 12, inhibition efficiency in HCl increased almost linearly with concentration up to 4.0%, followed by a smaller increment at 5.0%. The regression analysis showed an excellent linear fit with $R^2 = 0.9806$, indicating a strong correlation between silica concentration and inhibition efficiency in acidic media. This trend suggests that the coating grows progressively denser and more protective with increasing silica content, though a saturation effect begins to appear beyond 4.0%.

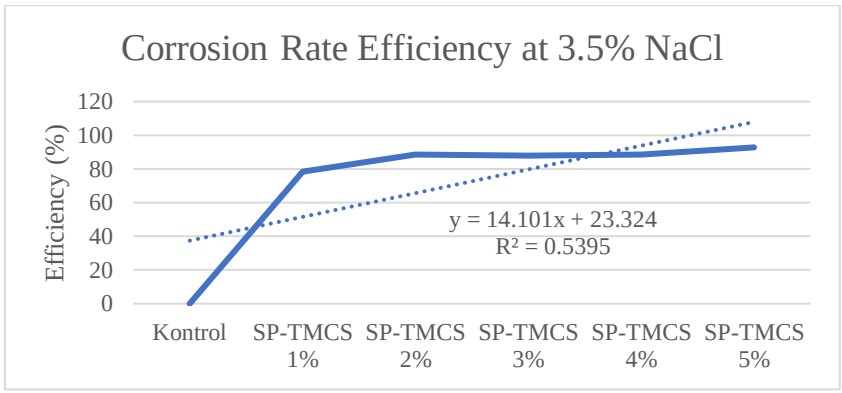

Fig. 13. Corrosion inhibition efficiency (%) of silica–TMCS coatings in 3.5% NaCl solution.

In contrast, Fig. 13 shows inhibition efficiency in NaCl rising sharply from 0% to 78.45% at 1.0% concentration, then gradually leveling off toward 92.82% at 5.0%. The regression fit yielded a lower $R^2 = 0.5395$, reflecting non-linear behavior due to the rapid formation of a protective barrier at low concentrations. This suggests that in saline media, even minimal silica–TMCS loading is sufficient to form an effective hydrophobic layer, while higher concentrations only provide incremental benefits.

3.7 Correlation Between Superhydrophobicity and Corrosion Protection

A clear relationship was established between the degree of surface superhydrophobicity and the corrosion inhibition efficiency of the silica–TMCS coatings. As demonstrated by contact angle measurements, coatings derived from rice husk silica (RHS) achieved the highest value of 153.1° at 3.0% concentration, followed by corncob silica (CCS, 150.8°) and sugarcane bagasse silica (SBS, 148.6°). These values confirm that RHS and CCS successfully reached the superhydrophobic threshold (CA ≥ 150°), whereas SBS remained slightly below this level.

Superhydrophobic surfaces, characterized by contact angles ≥150° and sliding angles ≤10°, are known to establish robust thermodynamic barriers against liquid adhesion. At the micro/nanoscale, the coatings generate a hierarchical roughness that traps air beneath water droplets, thereby supporting the Cassie–Baxter wetting state. In this regime, droplets rest on composite air–solid interfaces, which drastically limits the effective solid–liquid contact area and prevents electrolyte penetration into the substrate.

The strong correlation between wetting behavior and corrosion performance is supported by inhibition data. At 3.0% RHS, the corrosion rate was reduced from 190.95 mpy (control) to 37.42 mpy in 15% HCl and from 29.59 mpy to 2.13 mpy in 3.5% NaCl, corresponding to inhibition efficiencies of 80.4% and 92.8%, respectively. These results confirm that enhanced superhydrophobicity directly translates into improved corrosion resistance by impeding both water adsorption and ion transport at the coating–solution interface.

Nevertheless, increasing silica concentration beyond 4.0% caused a slight decline in performance. For instance, the CA of RHS dropped to 148.3° at 5.0%, falling below the superhydrophobic threshold, while inhibition efficiency plateaued in NaCl and declined slightly in HCl. This phenomenon can be attributed to particle agglomeration and increased solution viscosity, which lead to uneven coating morphology and micro-defects. Such irregularities compromise the uniformity of the protective layer, providing localized pathways for corrosive ion ingress.

Taken together, these findings highlight that both surface chemistry (Si–CH_3 substitution) and coating morphology (uniform micro/nanostructure) play decisive roles in achieving durable corrosion protection. An optimal balance is obtained at 3.0–4.0% silica concentration, where coatings exhibit maximum superhydrophobicity, minimal defect density, and high inhibition efficiency in both acidic and saline environments.

4. Conclusions

This study successfully demonstrated the valorization of agricultural biomass wastes (rice husk, corncob, and sugarcane bagasse) into high-purity silica, which was further functionalized with trimethylchlorosilane (TMCS) to produce superhydrophobic coatings. Among the sources, rice husk silica (RHS) achieved the highest yield (95.41%) and structural quality, as confirmed by FTIR and XRD analyses. Surface modification effectively converted hydrophilic silanol groups into nonpolar Si–CH_3 and Si–C functionalities, enabling the formation of coatings with excellent water repellency. Ultrasonic dip-coating produced uniform films, with RHS-based coatings at 3.0–4.0% concentration exhibiting contact angles above 150° and sliding angles below 10°, meeting the criteria for superhydrophobicity. Corrosion tests in 15% HCl and 3.5% NaCl media

showed substantial protection, with inhibition efficiencies reaching 92.82% and a clear correlation between hydrophobicity and corrosion resistance. However, excessive silica loading (>4.0%) reduced coating uniformity due to particle agglomeration. Overall, these findings highlight biomass-derived silica as a sustainable, cost-effective, and high-performance material for advanced anti-corrosion applications.

Acknowledgments.

The authors acknowledge the financial support from Universitas Negeri Medan through the PNBP Research Fund. Technical assistance from the Faculty of Mathematics and Natural Sciences is also gratefully acknowledged.

References

[1] Harsimran, S., Santosh, K., Rakesh, K.: Overview of corrosion and its control: A critical review. Faculty of Engineering, University of Kragujevac. (2021) doi: 10.24874/PES03.01.002

[2] Kuruvila, R., Thirumalai Kumaran, S., Khan, M.A., Uthayakumar, M.: A brief review on the erosion-corrosion behavior of engineering materials. Corrosion Reviews. Vol. 36, No. 5, pp. 435–447 (2018)

[3] Sinaga, A.J., Simanjuntak, S.L.M.H., Manurung, C.S.P.: Analisa laju korosi dan kekerasan pada stainless steel 316L dalam larutan 10% NaCl dengan variasi waktu perendaman. (2020)

[4] Farag, A.A.: Applications of nanomaterials in corrosion protection coatings and inhibitors. Corrosion Reviews. De Gruyter Open Ltd. (Feb 2020) doi: 10.1515/corrrev-2019-0011

[5] Chobaomsup, V., Metzner, M., Boonyongmaneerat, Y.: Superhydrophobic surface modification for corrosion protection of metals and alloys. Journal of Coatings Technology and Research. Vol. 17, No. 3 (2020) doi: 10.1007/s11998-020-00327-2

[6] Jurak, S.F., Jurak, E.F., Uddin, M.N., Asmatulu, R.: Functional superhydrophobic coating systems for possible corrosion mitigation. International Journal of Automation Technology. Fuji Technology Press. (2020) doi: 10.20965/ijat.2020.p0148

[7] Farag, A.A., Mohamed, E.A., Toghan, A.: The new trends in corrosion control using superhydrophobic surfaces: A review. Corrosion Reviews. Vol. 41, No. 1 (2023) doi: 10.1515/corrrev-2022-0020

[8] Zeng, Q., et al.: Durable superhydrophobic silica/epoxy resin coating for the enhanced corrosion protection of steel substrates in high salt and H_2S environments. Colloids and Surfaces A: Physicochemical and Engineering Aspects. Vol. 654 (2022) doi: 10.1016/j.colsurfa.2022.130137

[9] Albert, E., Cotolan, N., Nagy, G., Sáfrán, N., Szabó, G., Mureşan, L.M., Hórvölgyi, Z.: Mesoporous silica coatings with improved corrosion protection properties. Microporous and Mesoporous Materials. Vol. 201, pp. 102–113 (2015)

[10] Xu, Y., et al.: Anticorrosive behavior of epoxy coating modified with hydrophobic nano-silica on phosphatized carbon steel. Progress in Organic Coatings. Vol. 151 (2021) doi: 10.1016/j.porgcoat.2020.106051

[11] Silviana, S., Darmawan, A., Dalanta, F., Subagio, A., Hermawan, F., Santoso, H.M.: Superhydrophobic coating derived from geothermal silica to enhance material durability of bamboo using hexadimethylsilazane (HMDS) and trimethylchlorosilane (TMCS). *Materials (Basel)*. Vol. 14, No. 3, pp. 1–20 (2021) doi: 10.3390/ma14030530

[12] Heshmati, M.R., Amiri, S., Hosseini-Zori, M.: Synthesis and characterization of superhydrophobic-superoleophobic and anti-corrosion coatings via sol-gel process. *Open Journal of Organic Polymer Materials*. Vol. 10, pp. 1–15 (2020) doi: 10.4236/ojopm.101001
[13] Setiawan, W.K., Chiang, K.Y.: Crop residues as potential sustainable precursors for developing silica materials: A review. *Waste and Biomass Valorization*. Vol. 12, No. 5, pp. 2207–2236 (2021) doi: 10.1007/s12649-020-01126-x
[14] Lestari, Y.D., Rahayuningtyas, M.T., Utami, L.I., Wahyusi, K.N.: Sintesis silika xerogel dari sabut kelapa dengan metode sol-gel. *Jurnal Teknik Kimia*. Vol. 17, No. 2 (2023) doi: 10.33005/jurnal_tekkim.v17i2.3785
[15] Hidayat, R., Yupita, Pangestuti, P.W., Tafdila, N.A., Fabiani, V.A.: Ekstraksi dan karakterisasi silika dari abu limbah ampas tebu minuman sari tebu di Bangka. *Prosiding Seminar Nasional Sains dan Terapan*. Vol. 1, No. 1, pp. 72–77 (2023)
[16] Evan, Paradoyo, Darmawan, A.: Pembuatan nanosilika dari abu sekam padi pada variasi pH sol-gel. *Greensphere Journal of Environmental Chemistry*. Vol. 2, No. 1, pp. 8–13 (2022)
[17] Rahmi, R.: Sintesis silika alam dari kalsinasi sekam padi. *MASALIQ*. Vol. 4, No. 1, pp. 63–70 (2023) doi: 10.58578/masaliq.v4i1.2099
[18] Badan Pusat Statistik (BPS): Hasil Sensus Pertanian 2023. https://sensus.bps.go.id/ (2023)
[19] Fakir, S.H., Chaitanya Kumar, K., Ali, H., Rawat, J., Haq Farooqi, I.: Synthesis and evaluation of green corrosion inhibitor from rice husk to mitigate corrosion of carbon steel in NaCl environment. *Materials Today: Proceedings* (2023) doi: 10.1016/j.matpr.2022.11.147
[20] Wang, Q., et al.: Application of biomass corrosion inhibitors in metal corrosion control: A review. *Molecules*. (2023) doi: 10.3390/molecules28062832
[21] Hoo, D.Y., et al.: Ultrasonic cavitation: An effective cleaner and greener intensification technology in the extraction and surface modification of nanocellulose. *Ultrasonics Sonochemistry*. Vol. 90 (2022) doi: 10.1016/j.ultsonch.2022.106176
[22] Marín, R.R., Babick, F., Stintz, M.: Ultrasonic dispersion of nanostructured materials with probe sonication – practical aspects of sample preparation. *Powder Technology*. Vol. 318, pp. 451–458 (2017)
[23] Simanjuntak, C.T.N., et al.: Superhydrophobic silica ultrasonic coating based on Sinabung volcanic ash as anti-corrosion of ferrous metal materials. (2024)
[24] Simatupang, L., et al.: Kinerja rasio silika-cat dengan metode dipcoating pada permukaan logam untuk penghambat laju korosi. *Journal of Science and Applied Technology*. Vol. 7, No. 1, p. 43 (2023) doi: 10.35472/jsat.v7i1.1311
[25] Fathurrahman, M., Suhendar, U., Iryani, A., Widiastuti, D., Ahmad, S.N., Juniar, E.: Sintesis dan karakterisasi komposit eugenol-silika gel dari abu tongkol jagung serta analisis antibakteri dan daya serap terhadap air. *ALCHEMY: Jurnal Penelitian Kimia*. Vol. 18, No. 1, pp. 10–18 (2022) doi: 10.20961/alchemy.18.1.47161.10-18